PHYSICS

Observation of slow relaxation due to Hilbert space fragmentation in strongly interacting Bose-Hubbard chains

Kantaro Honda[1]*, Yosuke Takasu[1], Shimpei Goto[2], Hironori Kazuta[3], Masaya Kunimi[4], Ippei Danshita[3], Yoshiro Takahashi[1]

While isolated quantum systems generally thermalize after long-time evolution, there are several exceptions defying thermalization. A notable mechanism of this nonergodicity is the Hilbert space fragmentation (HSF), where the Hamiltonian matrix splits into an exponentially large number of sectors due to the presence of nontrivial conserved quantities. Using ultracold gases, here, we experimentally investigate the one-dimensional Bose-Hubbard system with neither disorder nor tilt potential, which has been predicted to exhibit HSF caused by a strong interatomic interaction. Specifically, we analyze far-from-equilibrium dynamics starting from a charge density wave of doublons (atoms in doubly occupied sites) in a singlon- and doublon-resolved manner to reveal a slowing down of the relaxation in a strongly interacting regime. We find that the numbers of singlons and doublons are conserved during the dynamics, indicating HSF as a mechanism of the observed slow relaxation. Our results provide an experimental confirmation of the conserved quantities responsible for HSF.

INTRODUCTION

The problem of quantum thermalization, i.e., how isolated quantum many-body systems that undergo the reversible unitary time evolution can reach thermal equilibrium states, lies at the heart of modern quantum statistical physics and is of considerable recent interest. As a mechanism of the thermalization, the eigenstate thermalization hypothesis (ETH) is known, which states that expectation values of physical quantities for eigenstates of a quantum many-body system coincide with that of the microcanonical ensemble in the corresponding energy (*1*–*4*). In particular, when a quantum many-body system satisfies the strong version of the ETH, where all of the eigenstates satisfy the ETH, the long-time average of the physical quantity coincides with the microcanonical average, that is, the system thermalizes (*5*, *6*).

The remarkable progress of artificial quantum systems, such as ultracold gases, Rydberg atom arrays, trapped ions, and superconducting qubits, has enabled indispensable studies on the problem of the thermalization from both experimental and theoretical sides. In better understanding of the mechanisms of the thermalization, investigating nonergodic systems, which do not show thermalization, is important. Illustrative examples of nonergodic systems include integrable (*7*–*12*) and many-body localized (MBL) systems (*13*–*27*), where thermalization is prevented because of the presence of an extensive number of conserved quantities and the strong disorder potential, respectively. Furthermore, the recent findings of another type of nonergodic systems show the diversity of origins of nonergodic behavior, as exemplified by quantum many-body scar (*28*–*37*), stark MBL (*38*–*42*), and Hilbert space fragmentation (HSF) (*43*–*50*).

In particular, HSF typically results from the presence of nontrivial conserved quantities, leading to strong kinetic constraints on the system. Under these constraints, the Hilbert space is fragmented into an exponentially large number of disconnected subsectors (Krylov subsectors), where the dynamics are restricted to only a few subsectors, causing the system not to thermalize. Experimentally, the nonergodic dynamics due to the HSF have been observed, especially in the one-dimensional (1D) Fermi-Hubbard system (*45*, *46*) and the 2D Bose-Hubbard system (*50*), where linear potential gradients (tilt potentials) are applied, and the total atom number and dipole moment are conserved. Theoretically, a disorder-free 1D Bose-Hubbard model with no trapping potential (*51*, *52*) and with a trapping potential (*40*, *53*, *54*) has been studied. In particular, in (*54*), it has been reported that the nonergodic behavior emerges in the strongly interacting regime when the dynamics start from a period-two charge density wave (CDW) of doublons (atoms in doubly occupied sites) (see Fig. 1, A and B), while rapid relaxation occurs starting from that of singlons. In this system, in addition to the total atom number, the numbers of doublons and singlons are emergent conserved quantities in the strongly interacting regime, which gives rise to strong HSF.

In this work, using ultracold Bose gases in optical lattices, we explore the role of interatomic interaction in the nonequilibrium dynamics following the sudden quench of the optical lattice depth, starting from a particular initial state of a period-two CDW of doublons with a small portion of singlons in a 1D disorder-free Bose-Hubbard system with no tilt potential (see Fig. 1A). We experimentally observe a notable difference between the quench dynamics starting from this type of initial state and that from the period-two CDW of singlons. The systematic measurement of the imbalance in a singlon- and doublon-resolved manner with varying the ratio of the interatomic interaction to the hopping energy reveals a slowing down of the relaxation of the imbalance of the doublons in a strongly interacting regime, in stark contrast with the behavior of the singlons, which exhibit the considerable relaxation in all interaction strengths. We find that both numbers of singlons and doublons are conserved during the quench dynamics, indicating the HSF as a mechanism of the observed slow relaxation. The interplay between the effects of parabolic potentials and interatomic interaction plays a role in the observed relaxation dynamics,

[1]Department of Physics, Graduate School of Science, Kyoto University, Kyoto 606-8502, Japan. [2]Institute for Liberal Arts, Institute of Science Tokyo, Ichikawa, Chiba 272-0827, Japan. [3]Department of Physics, Kindai University, Higashiosaka, Osaka 577-8502, Japan. [4]Department of Physics, Tokyo University of Science, Shinjuku, Tokyo 162-8601, Japan.
*Corresponding author. Email: honda.kantaro.35m@st.kyoto-u.ac.jp

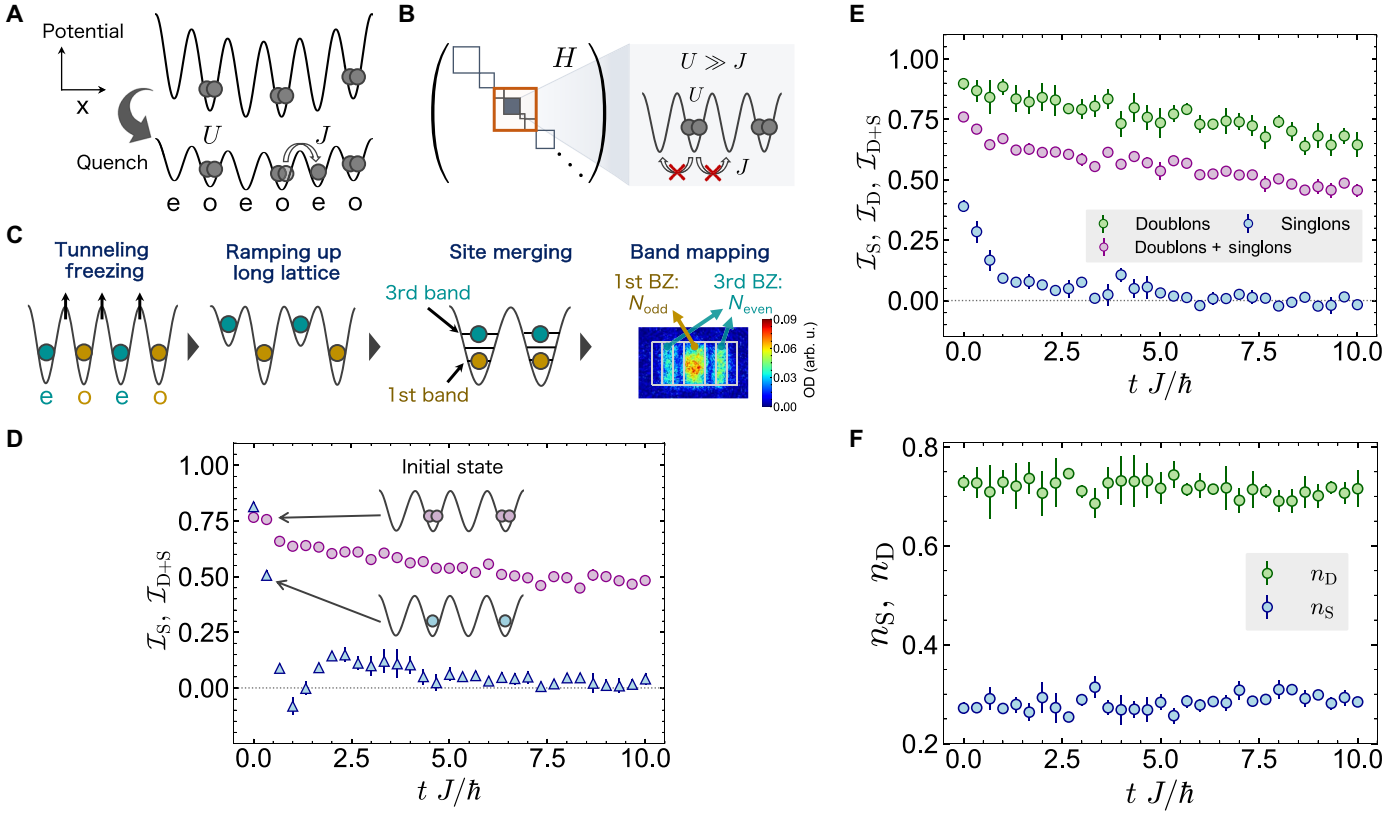

Fig. 1. Schematic of the experimental setup and illustration of observed quench dynamics. (**A**) Schematic of the 1D Bose-Hubbard model. (**B**) Schematic illustration of HSF. The orange square shows a subspace characterized by the particle number. This subspace is further fragmented into an exponentially large number of subsectors (Krylov subsectors) under some kinetic constraints, where the breakup of doublons into singlons is suppressed for $U \gg J$. (**C**) Schematic illustration of the sequence for a site mapping technique to measure the atom number imbalance. (**D**) Comparison of quench dynamics at $U/J = 52$ starting from $\hat{\rho}_{\mathrm{CDW(d,s)}}(0)$ (purple circle) and $\hat{\rho}_{\mathrm{CDW(s)}}(0)$ (blue triangle) as a function of the normalized holding time, with a tunneling time of $\hbar/J = 2.6$ ms along the direction of the 1D chains. Error bars in $\mathcal{I}_{\mathrm{D+S}}$ and $\mathcal{I}_{\mathrm{S}}$ show the SD of three and five independent scans, respectively. (**E**) Typical imbalance dynamics. (**F**) Typical dynamics of atom number fractions of doublons (n_{D}; green) and singlons (n_{S}; blue) as a function of the normalized holding time, with a tunneling time of $\hbar/J = 2.1$ ms along the direction of the 1D chains. In (E) and (F), all data are obtained at $U/J = 67$. Error bars for $\mathcal{I}_{\mathrm{S}}$ and $\mathcal{I}_{\mathrm{S}}$ in (E) show the SD of three independent scans, and those for $\mathcal{I}_{\mathrm{D}}$ in (E) and $n_{\mathrm{S/D}}$ in (F) show the SD calculated by the error propagation formula. OD, optical density; arb. u., arbitrary units.

which is reproduced by our theoretical calculation. In particular, we reveal the enhanced slowing down of the relaxation for doublons by partial removal of singlons that accelerate the equilibration of the imbalance through tunneling with no energy cost, which offers important insights into the quantum thermalization dynamics. We note that, in contrast to the pioneering work (*55*), where the atom number stability of the doublon itself, i.e., repulsively bound pair, prepared in an approximately isolated form (filling of doublons is typically 0.3) is observed, the present work reveals the nonequilibrium dynamics for interacting many-body systems of the doublons by observing the atom number imbalance between the odd and even sites.

RESULTS

Experimental setup

We start with the preparation of a ^{174}Yb Bose-Einstein condensate by evaporative cooling with the total atom number of about 1.3×10^4. A Mott insulating state of unit filling is formed after the atom loading into a 3D optical lattice, with a deep potential depth of $30E_{\mathrm{R}}$, where $E_{\mathrm{R}} = \hbar^2 k_{\mathrm{L}}^2/(2m)$ is the recoil energy of the optical lattice, $k_{\mathrm{L}} = 2\pi/\lambda_{\mathrm{short}}$ with $\lambda_{\mathrm{short}} = 532$ nm is the wave number of the laser for the optical lattice, and $\hbar$ is the Planck constant divided by 2π. Here, the preparation of the initial state of period-two CDW of doublons, i.e., $|\psi(0)\rangle_{\mathrm{CDW(d)}} = |\ \cdots\ 2020\ \cdots\rangle$ state in 1D chains, proceeds with the optical superlattice in the direction of 1D chains consisting of short ($\lambda_{\mathrm{short}} = 532$ nm) and long ($\lambda_{\mathrm{long}} = 1064$ nm) lattices (see section S1 for details of the loading procedure). For representing the many-body state of a 1D chain with M sites, here, we use the Fock basis

$$|n_1\ n_2\ \cdots\ n_M\rangle \equiv \bigotimes_{i=1}^{M} |n_i\rangle_i \qquad (1)$$

where $|n_i\rangle_i$ denotes the local Fock state at a site i with an atom number n_i. The central 1D chains of the atoms have a length of about 25. We note that in a prepared initial state, 25 to 30% of total atoms are singly occupied, which is confirmed by the remaining fraction of the atoms after the irradiation of a photoassociation (PA) laser. This is induced by the presence of low-density regions at the trap edges and the nonadiabaticity in the loading process (see section S1 for the estimation of the singlon fraction in the initial state).

After the initial state preparation, we perform a sudden quench by rapidly decreasing the potential depth to initiate the dynamics

along the 1D chains (Fig. 1A; see also the Materials and Methods for details of the quench procedure). The dynamics during the hold time in the 1D chains is described by the 1D Bose-Hubbard model, and the Hamiltonian is given by

$$\hat{H} = -J \sum_{\langle i,j \rangle} \hat{a}_i^\dagger \hat{a}_j + \frac{U}{2} \sum_{i=1}^{M} \hat{n}_i (\hat{n}_i - 1) + \sum_{i=1}^{M} V_i \hat{n}_i \quad (2)$$

where $\hat{a}_i \left(\hat{a}_i^\dagger \right)$ is the annihilation (creation) operator of a boson at a site i, J is the tunneling amplitude between nearest-neighbor sites $\langle i,j \rangle$, $\hat{n}_i \equiv \hat{a}_i^\dagger \hat{a}_i$ is the number operator at a site i, U is the on-site interaction strength, $V_i \equiv \Omega \left[i - (M+1)/2 \right]^2$ is the parabolic potential, and Ω is the strength of the parabolic potential (*54*). Here, we note that there is no tilt potential in Eq. 2, different from previous experimental studies of nonergodic dynamics due to the HSF (*45*, *46*, *50*) and the many-body scarring (*35*). Note that the relative strength of the parabolic potential Ω to the tunneling amplitude J depends on the lattice depth (see tables S1 and S2 for specific values of Ω / J), and Ω is small compared with hopping J of the singlon but not with that of the doublon.

To detect the atom distribution after the quench, we freeze the dynamics by rapidly ramping up the potential depth along the 1D chains. In this work, we focus on two physical quantities that characterize the atom distribution: atom number imbalance $\mathcal{I}(t)$ between the odd and even sites, and doublon- and singlon-resolved atom number fraction (n_D, n_S). The imbalance $\mathcal{I}(t)$ is defined as

$$\mathcal{I}(t) \equiv \frac{N_\mathrm{odd}(t) - N_\mathrm{even}(t)}{N_\mathrm{odd}(t) + N_\mathrm{even}(t)} \quad (3)$$

which becomes zero for thermalized states, where $N_\mathrm{odd}(t)$ and $N_\mathrm{even}(t)$ are the atom numbers in the odd and even sites, respectively. The measurement of the imbalance is performed by a site mapping technique, i.e., mapping of the even and odd sites to the first and third bands, respectively, followed by band mapping (see Fig. 1C and Materials and Methods for details of the imbalance measurement) (*45*, *46*, *56*, *57*). Note that, as we mention in the state preparation, the prepared state is not a pure state $|\psi(0)\rangle_\mathrm{CDW(d)}$ but a mixed state $\hat{\rho}_\mathrm{CDW(d,s)}(0)$, which involves singlons with 25 to 30% of total atoms. By exploiting the PA resonance that selectively excites and thus removes the doublons, we achieve measurements of the imbalance in a singlon- and doublon-resolved manner (*46*, *57*). Specifically, we measure the imbalance with and without the PA laser irradiation just after freezing of the dynamics and before site mapping, where the imbalance of singlons ($\mathcal{I}_\mathrm{w/PA} = \mathcal{I}_\mathrm{S}$) and that of both doublons and singlons ($\mathcal{I}_\mathrm{w/oPA}$) are obtained, respectively. Then, we obtain the imbalance of doublons ($\mathcal{I}_\mathrm{D}$) from the former two measured values as follows

$$\mathcal{I}_\mathrm{D} = \frac{\mathcal{I}_\mathrm{w/oPA} \cdot N_\mathrm{w/oPA} - \mathcal{I}_\mathrm{w/PA} \cdot N_\mathrm{w/PA}}{N_\mathrm{w/oPA} - N_\mathrm{w/PA}} \quad (4)$$

where $N_\mathrm{w/PA}$ ($N_\mathrm{w/oPA}$) is the atom number measured with (without) PA laser irradiation. The doublon- and singlon-resolved atom number fraction, n_D and n_S, is obtained with the atom numbers measured with and without the PA laser irradiation, $N_\mathrm{w/PA}$ and $N_\mathrm{w/oPA}$, as follows

$$n_\mathrm{S} = N_\mathrm{w/PA} / N_\mathrm{w/oPA} \quad (5)$$

$$n_\mathrm{D} = \left(N_\mathrm{w/oPA} - N_\mathrm{w/PA} \right) / N_\mathrm{w/oPA} \quad (6)$$

Note that these atom number fractions are important to characterize the nonequilibrium dynamics in the sense that they are emergent conserved quantities in the strongly interacting regime of the Bose-Hubbard chain, leading to the HSF (*54*).

Typical quench dynamics: Slow imbalance relaxation and doublon and singlon fraction conservation

We first show the comparison of the relaxation behavior obtained at $U/J = 67$ starting from the $\hat{\rho}_\mathrm{CDW(d,s)}(0)$ and $\hat{\rho}_\mathrm{CDW(s)}(0)$ states in Fig. 1D [see section S2 for details of the quench dynamics starting from the $\hat{\rho}_\mathrm{CDW(s)}(0)$ state]. Here, $\hat{\rho}_\mathrm{CDW(s)}(0)$ denotes an initial mixed state that is, in reality, created when we try to ideally prepare

$$|\psi(0)\rangle_\mathrm{CDW(s)} = |\cdots 1010 \cdots\rangle \quad (7)$$

In Fig. 1D, the imbalance $\mathcal{I}$ shows slow relaxation and remains far from zero, at least up to 10 times of the tunneling time along the 1D chains when the initial state is $\hat{\rho}_\mathrm{CDW(d,s)}(0)$, while the imbalance shows rapid relaxation and an oscillating behavior across zero when the initial state is $\hat{\rho}_\mathrm{CDW(s)}(0)$. These different relaxation behaviors are theoretically discussed in (*54*), where the nonergodic dynamics is expected when the initial state is $|\psi(0)\rangle_\mathrm{CDW(d)} = |\cdots 2020 \cdots\rangle$. Note that although the relaxation behavior in the 1D Bose-Hubbard system when the initial state is approximately $|\cdots 1010 \cdots\rangle$ has already been reported (*58*), we revisit this situation to show a clear difference in the quench dynamics depending on the initial states.

In the following, for the quantitative study, we focus on the quench dynamics starting from the $\hat{\rho}_\mathrm{CDW(d,s)}(0)$ state. In Fig. 1E, we show the typical quench dynamics of the imbalances of both doublons and singlons ("doublons + singlons," $\mathcal{I}_\mathrm{D+S}$), singlons ("singlons," $\mathcal{I}_\mathrm{S}$), and doublons ("doublons," $\mathcal{I}_\mathrm{D}$) obtained from the former two by Eq. 4, where $U/J = 67$. Here, the imbalances of doublons and singlons show slow and rapid relaxation, respectively. Note that tunneling time along the direction perpendicular to the 1D chains is $\hbar / \left(4J_\perp \right) = 92$ ms, about 3.5 times longer than the maximum measurement time. In addition to the successful observation of the slow relaxation behavior for doublons, we observe that both atom number fractions of doublons (n_D) and singlons (n_S) are almost conserved, as shown in Fig. 1F. This reveals that the atom numbers of both doublons and singlons serve as approximate conserved quantities, which is a key finding in the sense that this strongly supports the occurrence of HSF in our system, where the dissociation of doublons due to single particle tunnelings is suppressed for $U \gg J$ due to energy mismatch (see Fig. 1B). We note that the difference between the mechanism of HSF in the tilted systems of the previous studies and that in our system with no tilt is in nontrivial emergent conserved quantities that cause HSF. This conserved quantity is the dipole moment in addition to the total number of particles in the previous study with tilt, while in our system, it is the number of doublons and singlons in a strongly interacting regime in addition to the total number of particles. We find that the magnitude of Δ / U in this study is much smaller than one, where Δ is the maximum energy offset between neighboring sites in the parabolic trap in our system (see tables S1 and S2 for specific values of Δ / U). Therefore, our study is not in the region of $\Delta / U \gtrsim 1$, where HSF is caused by tilt potential, as in previous studies. From these

discussions, we also note that the HSF of our system is not sensitive to the system size, since the kinetic constraint comes mainly from the strong interaction rather than the trapping potential (*54*).

Dependency of quench dynamics on *U/J*

To elucidate the role of interatomic interaction and the interplay with the parabolic potential in the nonequilibrium dynamics, we investigate the dependency of the quench dynamics on the interaction strength U/J and the parabolic trap strength Ω/J by changing the potential depth along the 1D chains after the quench, shown in Fig. 2 (A to C). Here, in Fig. 2 (A and B), we observe an overall tendency of slower relaxation of the imbalance of doublons for larger U/J, while the imbalance of singlons shows fast relaxation, roughly independent of U/J. At the same time, in Fig. 2C, we observe that the atom number fractions of both doublons and singlons are almost conserved regardless of the value of U/J (see also Fig. 2E). These results can be understood intuitively as follows: Recall that the dissociation of a doublon into two singlons is approximately forbidden, as assured by the conservation of the fractions. In the cases of relatively small U/J, not only singlons can tunnel to adjacent vacant sites with the tunneling rate of J but also doublons via the process of the second-order perturbation, with an effective tunneling rate of

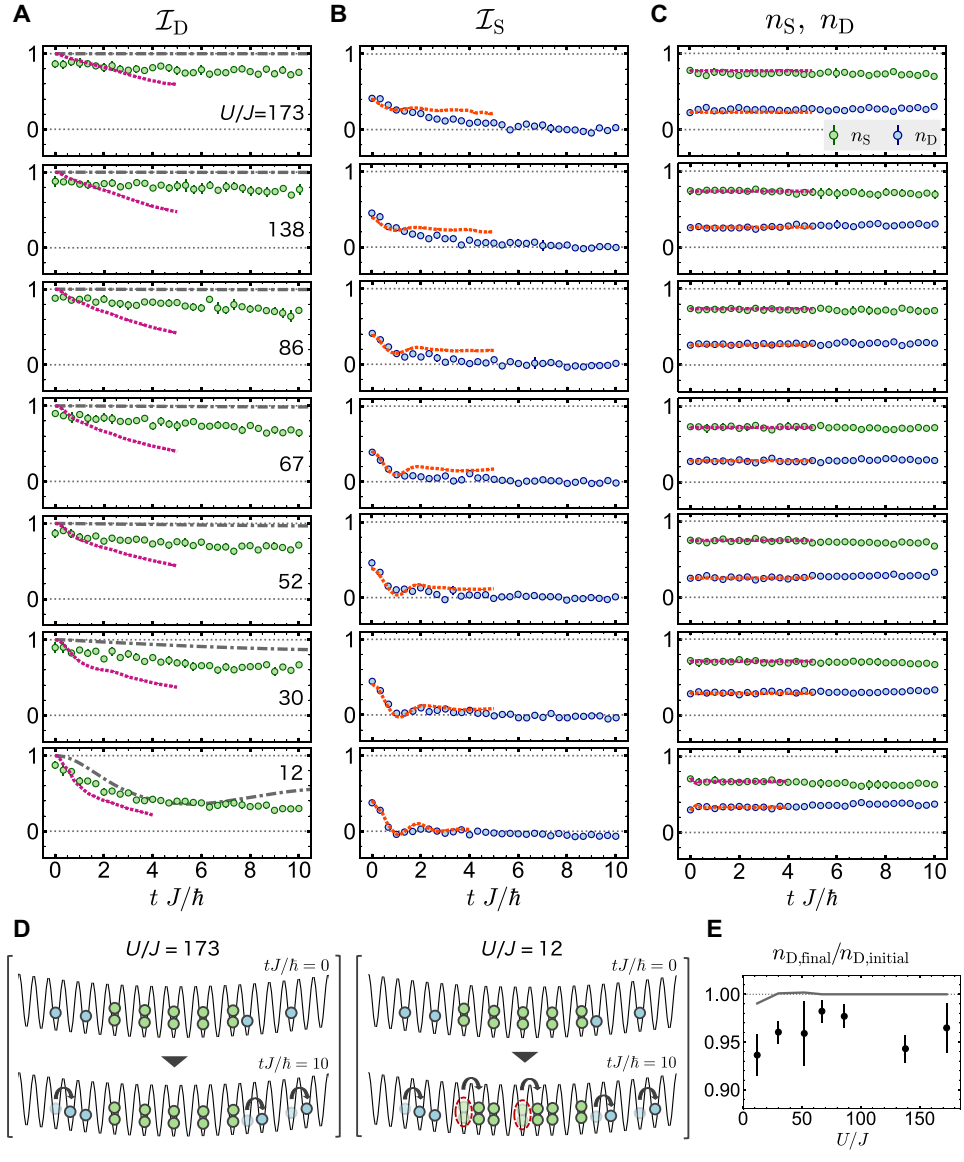

Fig. 2. Dependence of quench dynamics on *U/J*. (**A** to **C**) Imbalance dynamics of (A) doublons ($\mathcal{I}_D$), (B) singlons ($\mathcal{I}_S$), and (C) atom number fractions of doublons (n_D; green) and singlons (n_S; blue) on U/J. Error bars in (A) to (C) representing the SD are mostly smaller than symbols. In (A) to (C), dotted curves show the calculated values. In (A), dash-dotted curves show the calculated values for hardcore bosons as a reference (see Fig. 3 for details). Error bars of calculated values representing the statistical error are smaller than the dots of the curves. (**D**) Schematic illustration of tunneling dynamics of doublons and singlons in a lattice for relatively small (right) and large (left) U/J cases. (**E**) Change of the doublon fraction during the hold time. Here, the ratio of the averaged doublon fraction in $tJ/\hbar = 9 - 10$ ($n_{D,final}$) to that in $tJ/\hbar = 0 - 1$($n_{D,initial}$) is plotted. Error bars show the SD, which is calculated by the error propagation formula with the SD of the averaged doublon fractions $n_{D,initial}$ and $n_{D,final}$. The solid curve shows the ratio of the calculated averaged doublon fraction in $tJ/\hbar = 4 - 5$ ($tJ/\hbar = 3 - 4$ only in the case of $U/J = 12$) ($n_{D,final}$) to that in $tJ/\hbar = 0 - 1$($n_{D,initial}$).

$J_{\mathrm{eff}} = 2J^2/U$, as depicted in Fig. 2D (right), on the one hand. The time constant of the correlated tunneling, $\hbar/(2J_{\mathrm{eff}})$ is $3\hbar/J$ for the smallest U/J case ($U/J = 12$), where the factor of 2 in front of J_{eff} means the number of nearest-neighboring sites along the chain direction. In the cases of relatively large U/J, on the other hand, the rate of the effective hopping of the doublon becomes quite small, corresponding to about one-/five-time hopping event during the maximum holding time for the largest U/J case ($U/J = 173$), and thus only singlon tunneling is allowed, as in Fig. 2D (left). Note that the effect of the parabolic trap also contributes to the suppression of the doublon tunneling, while this effect is considerably weaker for singlons.

Comparison between experiments and numerical calculations

To provide a reference to be compared with the experimental results, we compute the real-time dynamics of the 1D Bose-Hubbard model of Eq. 2 using the time-evolving block decimation (TEBD) method (*59*), which is based on the matrix-product state (MPS) representation of a quantum many-body state (*60*). For TEBD, we use a second-order Suzuki-Trotter decomposition of the time evolution operator and optimally choose the time step Δt within the range $0.005 \leq \Delta t\ J/\hbar \leq 0.025$, depending on the interaction strength U/J. We set the maximal bond dimensions of MPS to be 2000 such that the time duration accessible with the numerical calculations is as short as or even shorter than the half of that in the experiments. In section S5, we elaborate on our theoretical protocol of initial state preparation, imitating the experimental situation. In Fig. 2 (A to C), we show the direct comparison of measured and calculated values of doublon- and singlon-resolved imbalance ($\mathcal{I}_{\mathrm{D}}$ and $\mathcal{I}_{\mathrm{S}}$) and doublon and singlon fractions (n_{D} and n_{S}) for several values of U/J. The quantitative disagreement between the experiment and simulations for $\mathcal{I}_{\mathrm{D}}$ in Fig. 2 may come from the limitation of the simulation to completely reflect the entire adiabatic and nonadiabatic process of the initial state preparation in the experiment, which may well be in the nonthermal distribution of the singlons. One can see, however, that the experimental data are within the range of the two simulation results of the case where the thermal initial state is given in the manner described in section S5 and that where the initial state does not include the singlons at all as another extreme case.

Competition among doublon-doublon interactions, doublon-singlon interactions, and a parabolic trap in the imbalance dynamics

While we see the agreement between the experimental data and theoretical calculations, here, we discuss how much extent the experimental results can be understood in an intuitive manner and clarify the nontrivial feature beyond simple interpretations. Specifically, we first see whether we can understand, in a unified manner, the dynamics of the singlons and doublons by regarding both of them as simple, noninteracting hardcore bosons, with the corresponding effective tunneling amplitude $J_{\mathrm{eff}} = J$ for the singlons and $J_{\mathrm{eff}} = 2J^2/U$ for the doublons placed in a parabolic trap with the trap strength Ω, thus characterized only by $(\Omega/J_{\mathrm{eff}})_{\mathrm{S}} = \Omega/J$ $(\Omega/J_{\mathrm{eff}})_{\mathrm{D}} = (\Omega/J_{\mathrm{eff}})_{\mathrm{S}} \cdot (U/J)$, respectively. In Fig. 3, we show a comparison of the experimental results of the imbalance dynamics for the singlons for the initial $\hat{\rho}_{\mathrm{CDW(s)}}(0)$ state and those for the doublon for the initial $\hat{\rho}_{\mathrm{CDW(d,s)}}(0)$ state as a function of the time normalized by the effective tunneling amplitude J_{eff} [see also section S2 for the quench dynamics starting from a $\hat{\rho}_{\mathrm{CDW(s)}}(0)$ state]. Note that, because of the large difference in the amplitude of J_{eff} between the singlons and doublons, the parameter regions of $(\Omega/J_{\mathrm{eff}})_{\mathrm{S}}$ and $(\Omega/J_{\mathrm{eff}})_{\mathrm{D}}$ have no overlap. Here, instead of the direct comparison of the experimental data, as shown in Fig. 3C, we focus on the comparison of the experimental results for the doublons with the theoretical calculations for the singlons, with a parameter region of $(\Omega/J_{\mathrm{eff}})_{\mathrm{S}}$ beyond 0.44, in accord with that for the doublons. Because the calculation for the singlons is rather straightforward, and we see that the calculations well reproduce the experimental results for $(\Omega/J_{\mathrm{eff}})_{\mathrm{S}}$ below 0.23, as also shown in fig. S3, we well expect the validity of the calculations for the singlons also for $(\Omega/J_{\mathrm{eff}})_{\mathrm{S}}$ beyond 0.44, which should be compared with the experimental results for the doublons in the corresponding region of $(\Omega/J_{\mathrm{eff}})_{\mathrm{D}}$. While the slow, nonoscillatory relaxation behavior is commonly observed both for the experiments and the calculations in Fig. 3C, there is an overall discrepancy in that the experiments for the doublons show faster relaxation than the calculations. Note that the effective parabolic trap strengths of $(\Omega/J_{\mathrm{eff}})_{\mathrm{S}}$ in the calculation and $(\Omega/J_{\mathrm{eff}})_{\mathrm{D}}$ in the experiments are the same in this comparison. The result of the comparison thus indicates that the doublons in this experiment cannot be simply interpreted as the noninteracting hardcore bosons, and we need to take interaction effects into consideration for full understanding of the observed behaviors.

First, we consider an effective nearest-neighbor doublon-doublon interaction, which is described in the following effective Hamiltonian for $U/J \gg 1$ (*51*)

$$H^{\mathrm{eff}} = \frac{2J^2}{U} \sum_{\langle i,j \rangle} \left[-8\hat{S}_i^z \hat{S}_j^z + \left(\hat{S}_i^+ \hat{S}_j^- + \hat{S}_i^- \hat{S}_j^+ \right) \right] \tag{8}$$

where the doublon and holon (empty site) are associated to a fictitious spin up $|\uparrow_i\rangle$ and down $|\downarrow_i\rangle$, respectively, and $\hat{S}_i^z \equiv (|\uparrow_i\rangle\langle\uparrow_i| - |\downarrow_i\rangle\langle\downarrow_i|)/2$ and $\hat{S}_i^+ \equiv |\uparrow_i\rangle\langle\downarrow_i| = \left(\hat{S}_i^-\right)^\dagger$ are the spin-1/2 operators. Here, the first term on the right-hand side corresponds to the doublon-doublon interaction, which takes the same order of magnitude as that of the second term for the doublon hopping. This doublon-doublon interaction introduces the energy difference between the state of doublons in the CDW and the state that has doublons occupying in the nearest-neighboring sites, causing the slower relaxation of the initially prepared CDW of the doublons compared with the case of noninteracting hardcore bosons, in contrast to the observation in Fig. 3C.

Next, we consider the interaction between the doublons and singlons involved in the prepared initial $\hat{\rho}_{\mathrm{CDW(d,s)}}(0)$ state (see the situations depicted in Fig. 4A). While the tunneling process of $|2,0\rangle \leftrightarrow |1,1\rangle$ is suppressed for $U \gg J$, as shown in Fig. 4A (left), that of $|2,1\rangle \leftrightarrow |1,2\rangle$, shown in Fig. 4A (right), has no energy cost, causing the faster relaxation of the initially prepared CDW of the doublons, consistent with the observation in Fig. 3C. This behavior is also numerically confirmed, as shown in Fig. 4B, where we depict the time evolution of the atom density profile in a single Bose-Hubbard chain starting from the $|\psi(0)\rangle_{\mathrm{CDW(d)}} = |\cdots 2020 \cdots\rangle$ state (left) and $\hat{a}_{\mathrm{edge}}^\dagger |\psi(0)\rangle_{\mathrm{CDW(d)}} = |\cdots 2020 \cdots\rangle$ (right). Here, $\hat{a}_{\mathrm{edge}}^\dagger$ creates an atom at a site $i_{\mathrm{edge}} + 2$, where i_{edge} denotes the right-edge site of the initial doublon array. In the latter case, one singlon

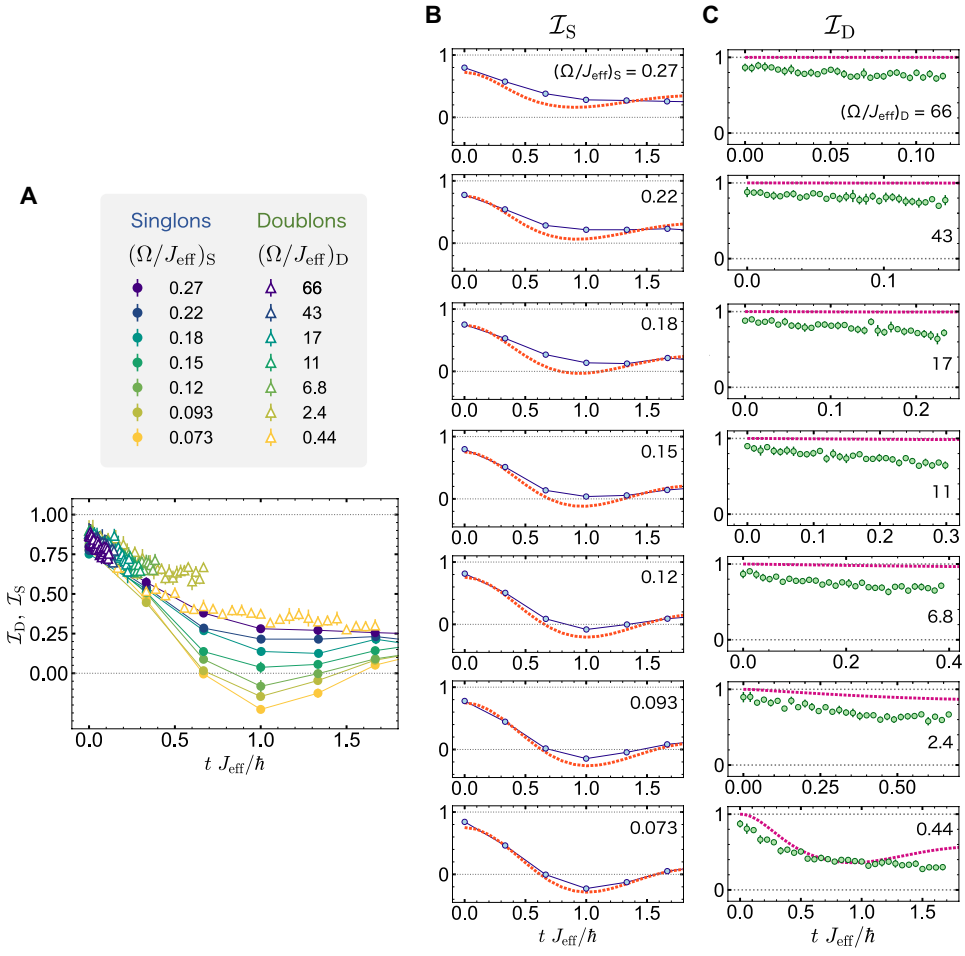

Fig. 3. Comparison of the measured imbalance dynamics of singlons starting from $\hat{\rho}_{\mathrm{CDW(s)}}(0)$ and those of doublons starting from $\hat{\rho}_{\mathrm{CDW(d,s)}}(0)$ with the numerical calculations. (**A**) Systematically measured imbalance dynamics of singlons (solid circles) and doublons (open triangles) for various $(\Omega/J_{\mathrm{eff}})_{\mathrm{D}}$ and $(\Omega/J_{\mathrm{eff}})_{\mathrm{S}}$. The horizontal axis represents the normalized time by the effective tunneling amplitude J_{eff}, where $J_{\mathrm{eff}} = J$ for singlons and $J_{\mathrm{eff}} = 2J^2/U$ for doublons. (**B** and **C**) Comparison of measured imbalance dynamics of (B) singlons and (C) doublons with the calculation for singlons (dotted curves) representing the case of noninteracting hardcore bosons. In the calculations of (B), the initial state is a mixed state $\hat{\rho}_{\mathrm{CDW(s)}}(0)$, while in (A), it is a pure state $|\psi\rangle_{\mathrm{CDW(s)}}(0)$. Error bars in (A) to (C) representing the SD are mostly smaller than symbols.

initially placed at the right edge of the trap moves to the trap center and disturbs ··· 2020 ··· configuration, which leads to a substantial decay of $\mathcal{I}_{\mathrm{D}}(t)$, as seen in the bottom of Fig. 4B. From these discussions, we attribute the disagreement between the experiment and the simulations based on the simple hardcore boson picture for $\mathcal{I}_{\mathrm{D}}$ in Fig. 3 to the interaction between singlons partially present in the initial state and doublons, as shown in Fig. 4A (right), highlighting the unique feature of the singlon-induced equilibration mechanism.

To experimentally confirm the effect of initially involved singlons on the quench dynamics, we prepare an initial $\hat{\rho}_{\mathrm{CDW(d,s)}}(0)$ state with a smaller singlon fraction by partially removing singlons with a selective ionization method, as depicted in Fig. 4C (see also section S4 for details of the removal scheme of singlons). In Fig. 4D, we show the imbalance dynamics of doublons starting from a $\hat{\rho}_{\mathrm{CDW(d,s)}}(0)$ state with and without the partial singlon removal as the open circle and the solid triangle, respectively. We observe the slower relaxation of imbalance of doublons in the case of a smaller singlon fraction in the initial state. In this way, we confirm the intriguing role of initially involved singlons in the quench dynamics, which qualitatively agrees with the numerical result.

DISCUSSION

In summary, we experimentally studied nonequilibrium dynamics of 1D Bose gases in optical lattices, which are well described as 2D arrays of independent Bose-Hubbard chains, after a sudden quench of the optical lattice depth. Starting from an initial period-two CDW state of doublons slightly mixed with singlons, we successfully observed slow relaxation in an imbalance measurement. We found that the numbers of both doublons and singlons are almost conserved during the dynamics, which strongly supports the occurrence of HSF. We also performed systematic measurements of quench dynamics for various U/J and the quantitative comparison of measured and calculated dynamics. In addition, we revealed the

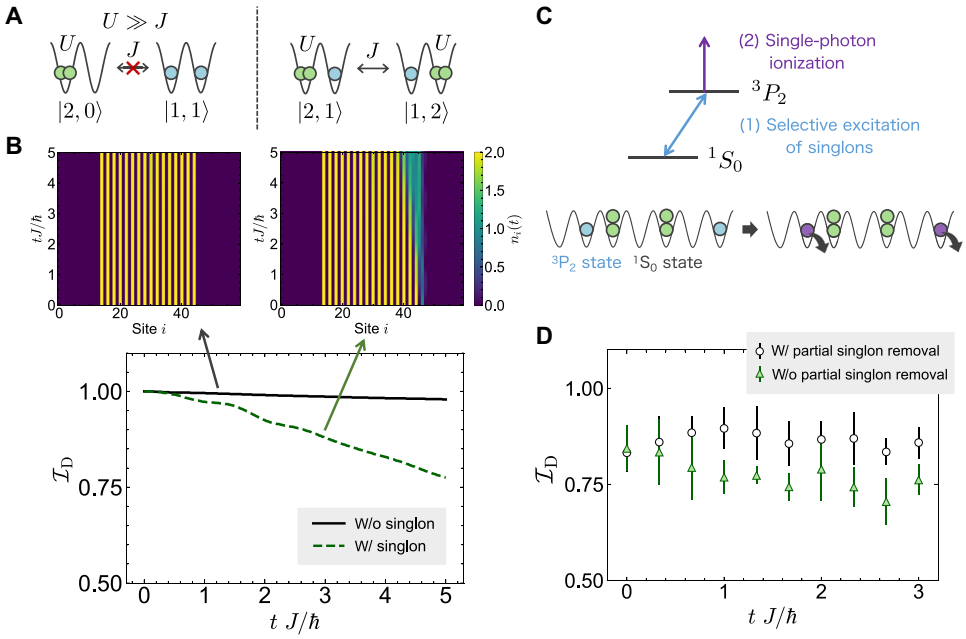

Fig. 4. Effect of singlons on the imbalance dynamics. (**A**) Schematic illustration of possible tunneling processes involving singlons between nearest-neighbor sites. (**B**) Calculated time evolution of the local density in the 1D Bose-Hubbard model (Eq. 2) for $U/J = 52$, starting from $|\psi(0)\rangle_{\mathrm{CDW(d)}} = |\cdots 2020 \cdots\rangle$ state (top left) and $\hat{a}^{\dagger}_{\mathrm{edge}}|\psi(0)\rangle_{\mathrm{CDW(d)}}$ state (top right), where one singlon is placed at the right edge of the trap in this case. Bottom: Imbalance dynamics of doublons ($\mathcal{I}_D$) obtained from the data in the top. (**C**) Schematic illustration of the removal procedure of only singlons from the initial $\hat{\rho}_{\mathrm{CDW(d,s)}}(0)$ state and the relevant energy levels. (**D**) Imbalance dynamics of doublons after partial removal of singlons in the initial $\hat{\rho}_{\mathrm{CDW(d,s)}}(0)$ state. Here, the plots of open circles and solid triangles show the results with ($n_S = 0.24$) and without ($n_S = 0.29$) the partial removal of singlons, respectively. Note that the loss of doublons in this measurement is negligibly small within the uncertainty. Both data are obtained at $U/J = 52$. All error bars show the SD.

effect of singlons involved in the initial $|\cdots 2020 \cdots\rangle$ state on the quench dynamics.

It is the time constant of hopping between 1D tubes that limits the observed timescale in our experiment. By limiting ourselves to a shorter observation time than this time constant, we safely provide a clear discussion by separating unnecessary factors that could cause deviations from the 1D system that we focus on in this study. The presence of singlons in the initial state of a period-two CDW of doublons causes the interaction between the doublon and singlon in the dynamics, which occurs on the timescale of the bare tunneling time. The doublon-singlon interaction results in richer dynamics already in the time window of less than 10 tunneling times, observed as a deviation from the noninteracting hardcore boson picture in doublon dynamics. Our system has enough room for improvement for a longer observation time. If we can further deepen the optical lattice in the direction perpendicular to the tube in our system, then we will be able to see dynamics for longer times. Here, because our lattice beams are not blue detuned, we do not have to worry about doublon lifetime, as in (*46*).

The successful preparation of arrays of dense doublons, i.e., $|\cdots 2020 \cdots\rangle$ state, and observations of dynamics of interacting doublons with a long lifetime open the possibility to study systems consisting of strongly interacting composite particles with ultracold gases. For instance, it is interesting to examine whether some exotic quantum many-body states formed by these composites can be experimentally realized, such as the pair superfluids of bosons (*61*), the η-pairing state of two-component (*62*) or multicomponent (*37*) fermions, and the quantum many-body scar states of bosons with a three-body constraint (*36*). More specifically, these states are expected to be prepared by adiabatically increasing the hopping from zero and controlling the energy offset of the double wells when one starts from the $|\cdots 2020 \cdots\rangle$ state. In addition, for the tilted 1D Bose-Hubbard system, previously studied (*35*), we expect that our measurement method of the dynamics of singlons and doublons in a singlon- and doublon-resolved manner may provide further insights into quench dynamics in that system.

MATERIALS AND METHODS

Sudden quench of the lattice depth

After the initial state preparation, we ramp up the potential depth in the directions perpendicular to the 1D chains from $s_L = [(30,\ 0),\ 30,\ 30]$ to $[(30,\ 0),\ 40,\ 40]$ in 1 ms and then perform a sudden quench to $s_L = \left[\left(s^{(x)}_{\mathrm{short}},\ 0\right),\ 40,\ 40\right]$ in 0.1 ms. Here, the tunneling time along the direction perpendicular to the 1D chains is 368 ms, and the effective tunneling time between chains, derived by dividing that tunneling time by four (the number of adjacent chains), is $\hbar/\left(4J_{\perp}\right) = 92$ ms. In the measurement of dependency of quench dynamics on U/J, the sweep time for quench is fixed to the above value independent of the potential depth along the 1D chains after the quench. Note that we numerically confirm that even when the change in the potential depth is maximal ($U/J = 12$ cases), the occupation probability of the ground state of the optical lattice potential after the quench exceeds 0.99, at least for singly occupied sites.

Atom number imbalance measurement

After we freeze the atom distribution by rapidly ramping up the potential depth along the 1D chains in 0.1 ms to $s^{(x)}_{\mathrm{short}} = 30$, we ramp up the long lattice to $s^{(x)}_{\mathrm{long}} = 40$ in 1 ms and then completely ramp down the short lattice in 1 ms. Here, we map the particle position, i.e., the odd and even sites, to the first and third bands of the potential of the long lattice, respectively (see Fig. 1C) (*57*). Then, the band mapping is performed in 0.6 ms, and we derive the imbalance $\mathcal{I}$ from the obtained band mapping image. Note that in our analysis, we count the atom numbers in the "first Brillouin zone (BZ) + half of the second BZ on the closer side to the first BZ" and "third BZ + half of the second BZ on the closer side to the third BZ" as N_{odd} and N_{even}, respectively, taking into account the possible imperfection of our band mapping process, although the second BZ population is small. We also note that we observe a slight deviation of imbalance from zero $[\mathcal{I}_{\mathrm{offset}} = 0.082(3)]$ when we start the quench dynamics from $|\cdots 1111 \cdots\rangle$ state as a reference state, which should show zero imbalance. This might be due to the imperfection of the particle position mapping or band mapping. In our analysis, we subtract this offset from the obtained imbalance $\mathcal{I}$. Imbalance of doublons, $\mathcal{I}_{\mathrm{D}}$, is calculated by Eq. 4, with calibrated values of $\mathcal{I}_{\mathrm{w/PA}}$ and $\mathcal{I}_{\mathrm{w/oPA}}$.

Supplementary Materials

This PDF file includes:

Sections S1 to S6
Figs. S1 to S6
Tables S1 and S2
References

REFERENCES AND NOTES

1. J. M. Deutsch, Quantum statistical mechanics in a closed system. *Phys. Rev. A* **43**, 2046–2049 (1991).
2. M. Srednicki, Chaos and quantum thermalization. *Phys. Rev. E* **50**, 888–901 (1994).
3. M. Rigol, V. Dunjko, M. Olshanii, Thermalization and its mechanism for generic isolated quantum systems. *Nature* **452**, 854–858 (2008).
4. J. M. Deutsch, Eigenstate thermalization hypothesis. *Rep. Prog. Phys.* **81**, 082001 (2018).
5. L. D'Alessio, Y. Kafri, A. Polkovnikov, M. Rigol, From quantum chaos and eigenstate thermalization to statistical mechanics and thermodynamics. *Adv. Phys.* **65**, 239–362 (2016).
6. T. Mori, T. N. Ikeda, E. Kaminishi, M. Ueda, Thermalization and prethermalization in isolated quantum systems: A theoretical overview. *J. Phys. B At. Mol. Opt. Phys.* **51**, 112001 (2018).
7. T. Kinoshita, T. Wenger, D. S. Weiss, A quantum Newton's cradle. *Nature* **440**, 900–903 (2006).
8. M. Rigol, V. Dunjko, V. Yurovsky, M. Olshanii, Relaxation in a completely integrable many-body quantum system: An ab initio study of the dynamics of the highly excited states of 1D lattice hard-core bosons. *Phys. Rev. Lett.* **98**, 050405 (2007).
9. M. Rigol, Breakdown of thermalization in finite one-dimensional systems. *Phys. Rev. Lett.* **103**, 100403 (2009).
10. M. Rigol, Quantum quenches and thermalization in one-dimensional fermionic systems. *Phys. Rev. A* **80**, 053607 (2009).
11. A. C. Cassidy, C. W. Clark, M. Rigol, Generalized thermalization in an integrable lattice system. *Phys. Rev. Lett.* **106**, 140405 (2011).
12. L. Vidmar, M. Rigol, Generalized gibbs ensemble in integrable lattice models. *J. Stat. Mech. Theory Exp.* **2016**, 064007 (2016).
13. I. V. Gornyi, A. D. Mirlin, D. G. Polyakov, Interacting electrons in disordered wires: Anderson localization and low-*T* transport. *Phys. Rev. Lett.* **95**, 206603 (2005).
14. D. M. Basko, I. L. Aleiner, B. L. Altshuler, Metal–insulator transition in a weakly interacting many-electron system with localized single-particle states. *Ann. Phys. Rehabil. Med.* **321**, 1126 (2006).
15. D. A. Huse, R. Nandkishore, V. Oganesyan, Phenomenology of fully many-body-localized systems. *Phys. Rev. B* **90**, 174202 (2014).
16. E. Altman, R. Vosk, Universal dynamics and renormalization in many-body-localized systems. *Annu. Rev. Condens. Matter Phys.* **6**, 383–409 (2015).
17. R. Nandkishore, D. A. Huse, Many-body localization and thermalization in quantum statistical mechanics. *Annu. Rev. Condens. Matter Phys.* **6**, 15–38 (2015).
18. M. Schreiber, S. S. Hodgman, P. Bordia, H. P. Lüschen, M. H. Fischer, R. Vosk, E. Altman, U. Schneider, I. Bloch, Observation of many-body localization of interacting fermions in a quasirandom optical lattice. *Science* **349**, 842–845 (2015).
19. J.-Y. Choi, S. Hild, J. Zeiher, P. Schauß, A. Rubio- Abadal, T. Yefsah, V. Khemani, D. A. Huse, I. Bloch, C. Gross, Exploring the many-body localization transition in two dimensions. *Science* **352**, 1547–1552 (2016).
20. P. Sierant, D. Delande, J. Zakrzewski, Many-body localization due to random interactions. *Phys. Rev. A* **95**, 021601 (2017).
21. P. Sierant, D. Delande, J. Zakrzewski, Many-body localization for randomly interacting bosons. *Acta Phys. Polon. A* **132**, 1707 (2017).
22. H. P. Lüschen, P. Bordia, S. Scherg, F. Alet, E. Altman, U. Schneider, I. Bloch, Observation of slow dynamics near the many-body localization transition in one-dimensional quasiperiodic systems. *Phys. Rev. Lett.* **119**, 260401 (2017).
23. P. Sierant, J. Zakrzewski, Many-body localization of bosons in optical lattices. *New J. Phys.* **20**, 043032 (2018).
24. F. Alet, N. Laflorencie, Many-body localization: An introduction and selected topics. *C. R. Phys.* **19**, 498–525 (2018).
25. D. A. Abanin, E. Altman, I. Bloch, M. Serbyn, Colloquium: Many-body localization, thermalization, and entanglement. *Rev. Mod. Phys.* **91**, 021001 (2019).
26. T. Kohlert, S. Scherg, X. Li, H. P. Lüschen, S. Das Sarma, I. Bloch, M. Aidelsburger, Observation of many-body localization in a one-dimensional system with a single-particle mobility edge. *Phys. Rev. Lett.* **122**, 170403 (2019).
27. P. Sierant, M. Lewenstein, A. Scardicchio, L. Vidmar, J. Zakrzewski, Many-body localization in the age of classical computing. *Rep. Prog. Phys.* **88**, 026502 (2025).
28. H. Bernien, S. Schwartz, A. Keesling, H. Levine, A. Omran, H. Pichler, S. Choi, A. S. Zibrov, M. Endres, M. Greiner, V. Vuletić, M. D. Lukin, Probing manybody dynamics on a 51-atom quantum simulator. *Nature* **551**, 579–584 (2017).
29. H. Zhao, J. Vovrosh, F. Mintert, J. Knolle, Quantum many-body scars in optical lattices. *Phys. Rev. Lett.* **124**, 160604 (2020).
30. M. Serbyn, D. A. Abanin, Z. Papić, Quantum manybody scars and weak breaking of ergodicity. *Nat. Phys.* **17**, 675–685 (2021).
31. D. Bluvstein, A. Omran, H. Levine, A. Keesling, G. Semeghini, S. Ebadi, T. T. Wang, A. A. Michailidis, N. Maskara, W. W. Ho, S. Choi, M. Serbyn, M. Greiner, V. Vuletić, M. D. Lukin, Controlling quantum manybody dynamics in driven rydberg atom arrays. *Science* **371**, 1355–1359 (2021).
32. Z. Papić, "Weak ergodicity breaking through the lens of quantum entanglement," in *Entanglement in Spin Chains: From Theory to Quantum Technology Applications* (Springer International Publishing, 2022), pp. 341–395.
33. S. Moudgalya, B. A. Bernevig, N. Regnault, Quantum many-body scars and Hilbert space fragmentation: A review of exact results. *Rep. Prog. Phys.* **85**, 086501 (2022).
34. A. Chandran, T. Iadecola, V. Khemani, R. Moessner, Quantum many-body scars: A quasiparticle perspective. *Annu. Rev. Condens. Matter Phys.* **14**, 443–469 (2023).
35. G.-X. Su, H. Sun, A. Hudomal, J.-Y. Desaules, Z.-Y. Zhou, B. Yang, J. C. Halimeh, Z.-S. Yuan, Z. Papić, J.-W. Pan, Observation of many-body scarring in a Bose-Hubbard quantum simulator. *Phys. Rev. Res.* **5**, 023010 (2023).
36. R. Kaneko, M. Kunimi, I. Danshita, Quantum manybody scars in the Bose-Hubbard model with a three-body constraint. *Phys. Rev. A* **109**, L011301 (2024).
37. M. Nakagawa, H. Katsura, M. Ueda, Exact eigenstates of multicomponent Hubbard models: SU(*N*) magnetic η pairing, weak ergodicity breaking, and partial integrability. *Phys. Rev. Res.* **6**, 043259 (2024).
38. M. Schulz, C. A. Hooley, R. Moessner, F. Pollmann, Stark many-body localization. *Phys. Rev. Lett.* **122**, 040606 (2019).
39. E. van Nieuwenburg, Y. Baum, G. Refael, From bloch oscillations to many-body localization in clean interacting systems. *Proc. Natl. Acad. Sci. U.S.A.* **116**, 9269–9274 (2019).
40. R. Yao, T. Chanda, J. Zakrzewski, Nonergodic dynamics in disorder-free potentials. *Ann. Phys. Rehabil. Med.* **435**, 168540 (2021).
41. W. Morong, F. Liu, P. Becker, K. Collins, L. Feng, A. Kyprianidis, G. Pagano, T. You, A. Gorshkov, C. Monroe, Observation of stark many-body localization without disorder. *Nature* **599**, 393 (2021).
42. Q. Guo, C. Cheng, H. Li, S. Xu, P. Zhang, Z. Wang, C. Song, W. Liu, W. Ren, H. Dong, R. Mondaini, H. Wang, Stark many-body localization on a superconducting quantum processor. *Phys. Rev. Lett.* **127**, 240502 (2021).
43. P. Sala, T. Rakovszky, R. Verresen, M. Knap, F. Pollmann, Ergodicity breaking arising from Hilbert space fragmentation in dipole-conserving hamiltonians. *Phys. Rev. X* **10**, 011047 (2020).
44. V. Khemani, M. Hermele, R. Nandkishore, Localization from Hilbert space shattering: From theory to physical realizations. *Phys. Rev. B* **101**, 174204 (2020).
45. S. Scherg, T. Kohlert, P. Sala, F. Pollmann, B. Hebbe Madhusudhana, I. Bloch, M. Aidelsburger, Observing non-ergodicity due to kinetic constraints in tilted Fermi-Hubbard chains. *Nat. Commun.* **12**, 4490 (2021).

46. T. Kohlert, S. Scherg, P. Sala, F. Pollmann, B. Hebbe Madhusudhana, I. Bloch, M. Aidelsburger, Exploring the regime of fragmentation in strongly tilted Fermi-Hubbard chains. *Phys. Rev. Lett.* **130**, 010201 (2023).
47. Y. Li, P. Sala, F. Pollmann, Hilbert space fragmentation in open quantum systems. *Phys. Rev. Res.* **5**, 043239 (2023).
48. Y.-Y. Wang, Y.-H. Shi, Z.-H. Sun, C.-T. Chen, Z.-A. Wang, K. Zhao, H.-T. Liu, W.-G. Ma, Z. Wang, H. Li, J.-C. Zhang, Y. Liu, C.-L. Deng, T.-M. Li, Y. He, Z.-H. Liu, Z.-Y. Peng, X. Song, G. Xue, H. Yu, K. Huang, Z. Xiang, D. Zheng, K. Xu, H. Fan, Exploring Hilbert-space fragmentation on a superconducting processor. *PRX Quantum* **6**, 010325 (2024).
49. L. Zhao, P. R. Datla, W. Tian, M. M. Aliyu, H. Loh, Observation of quantum thermalization restricted to Hilbert space fragments and Z_{2k} scars. *Phys. Rev. X* **15**, 011035 (2025).
50. D. Adler, D. Wei, M. Will, K. Srakaew, S. Agrawal, P. Weckesser, R. Moessner, F. Pollmann, I. Bloch, J. Zeiher, Observation of Hilbert space fragmentation and fractonic excitations in 2D. *Nature* **636**, 80–85 (2024).
51. G. Carleo, F. Becca, M. Schiró, M. Fabrizio, Localization and glassy dynamics of many-body quantum systems. *Sci. Rep.* **2**, 243 (2012).
52. A. Russomanno, M. Fava, R. Fazio, Nonergodic behavior of the clean Bose-Hubbard chain. *Phys. Rev. B* **102**, 144302 (2020).
53. R. Yao, J. Zakrzewski, Many-body localization of bosons in an optical lattice: Dynamics in disorder-free potentials. *Phys. Rev. B* **102**, 104203 (2020).
54. M. Kunimi, I. Danshita, Nonergodic dynamics of the one-dimensional Bose-Hubbard model with a trapping potential. *Phys. Rev. A* **104**, 043322 (2021).
55. K. Winkler, G. Thalhammer, F. Lang, R. Grimm, J. Hecker Denschlag, A. Daley, A. Kantian, H. Büchler, P. Zoller, Repulsively bound atom pairs in an optical lattice. *Nature* **441**, 853–856 (2006).
56. J. Sebby-Strabley, M. Anderlini, P. S. Jessen, J. V. Porto, Lattice of double wells for manipulating pairs of cold atoms. *Phys. Rev. A* **73**, 033605 (2006).
57. S. Fölling, S. Trotzky, P. Cheinet, M. Feld, R. Saers, A. Widera, T. Müller, I. Bloch, Direct observation of second-order atom tunnelling. *Nature* **448**, 1029–1032 (2007).
58. S. Trotzky, Y.-A. Chen, A. Flesch, I. P. McCulloch, U. Schollwöck, J. Eisert, I. Bloch, Probing the relaxation towards equilibrium in an isolated strongly correlated one-dimensional Bose gas. *Nat. Phys.* **8**, 325–330 (2012).
59. G. Vidal, Efficient simulation of one-dimensional quantum many-body systems. *Phys. Rev. Lett.* **93**, 040502 (2004).
60. U. Schollwöck, The density-matrix renormalization group in the age of matrix product states. *Ann. Phys.* **326**, 96 (2011).
61. A. J. Daley, J. M. Taylor, S. Diehl, M. Baranov, P. Zoller, Atomic three-body loss as a dynamical threebody interaction. *Phys. Rev. Lett.* **102**, 040402 (2009).
62. A. Kantian, A. J. Daley, P. Zoller, η Condensate of fermionic atom pairs via adiabatic state preparation. *Phys. Rev. Lett.* **104**, 240406 (2010).
63. M. Fishman, S. R. White, E. M. Stoudenmire, The ITensor software library for tensor network calculations. *SciPost Phys. Codebases* **4**, 1–53 (2022).
64. J. H. Denschlag, J. E. Simsarian, H. Häffner, C. McKenzie, A. Browaeys, D. Cho, K. Helmerson, S. L. Rolston, W. D. Phillips, A Bose-Einstein condensate in an optical lattice. *J. Phys. B At. Mol. Opt. Phys.* **35**, 3095–3110 (2002).
65. T. Tomita, S. Nakajima, I. Danshita, Y. Takasu, Y. Takahashi, Observation of the Mott insulator to superfluid crossover of a driven-dissipative Bose-Hubbard system. *Sci. Adv.* **3**, e1701513 (2017).
66. S. Kato, S. Sugawa, K. Shibata, R. Yamamoto, Y. Takahashi, Control of resonant interaction between electronic ground and excited states. *Phys. Rev. Lett.* **110**, 173201 (2013).
67. S. Kato, K. Inaba, S. Sugawa, K. Shibata, R. Yamamoto, M. Yamashita, Y. Takahashi, Laser spectroscopic probing of coexisting superfluid and insulating states of an atomic Bose–Hubbard system. *Nat. Commun.* **7**, 11341 (2016).
68. Y. Nakamura, Y. Takasu, J. Kobayashi, H. Asaka, Y. Fukushima, K. Inaba, M. Yamashita, Y. Takahashi, Experimental determination of Bose-Hubbard energies. *Phys. Rev. A* **99**, 033609 (2019).
69. O. Dutta, M. Gajda, P. Hauke, M. Lewenstein, D.-S. Lühmann, B. A. Malomed, T. Sowiński, J. Zakrzewski, Non-standard Hubbard models in optical lattices: A review. *Rep. Prog. Phys.* **78**, 066001 (2015).

Acknowledgments: We thank S. Taie, L. Asteria, and N. Navon for helpful discussions. We also thank Y. Nakamura for help for the 325-nm light. The MPS calculations in this work are performed with the ITensor library (*63*). **Funding:** This work was supported by the Grant-in-Aid for Scientific Research of JSPS [no. JP17H06138 (Y.Takah.), no. JP18H05405 (Y.Takah.), no. JP18H05228 (I.D. and Y.Takah.), no. JP21H01014 (I.D. and Y.Takas.), no. JP22H05268 (M.K.), and no. JP24KJ1332 (K.H.)], JST CREST [nos. JPMJCR1673 (I.D. and Y.Takah.) and JPMJCR23I3 (Y.Takah.)], MEXT Quantum Leap Flagship Program (MEXT Q-LEAP) [no. JPMXS0118069021 (I.D. and Y.Takah.)], JST Moonshot R&D Grant [no. JPMJMS2268 (Y.Takah.) and no. JPMJMS2269 (Y.Takah.)], JST FOREST [no. JPMJFR202T (I.D.)], and JST ASPIRE [no. JPMJAP24C2 (M.K., I.D., and Y.Takah.)]. **Author contributions:** K.H. and Y.Takas. carried out the experiments and data analysis. S.G., H.K., M.K., and I.D. carried out the theoretical calculation. Y.Takah. supervised the whole project. All authors contributed to the writing of the manuscript. **Competing interests:** The authors declare that they have no competing interests. **Data and materials availability:** All data needed to evaluate the conclusions in the paper are present in the paper and/or the Supplementary Materials.

Submitted 14 December 2024
Accepted 2 May 2025
Published 6 June 2025
10.1126/sciadv.adv3255